Kaposi's sarcoma-associated herpesvirus ORF68 is a DNA binding protein required for viral genome cleavage and packaging

Matthew R Gardner[a], and Britt A Glaunsinger[a,b,c,#]

[a] Division of Infectious Diseases and Immunity, School of Public Health, University of California Berkeley, CA, USA

[b] Department of Plant & Microbial Biology, University of California Berkeley, CA, USA

[c] Howard Hughes Medical Institute, Chevy Chase, MD, USA

[#]Corresponding Author: glaunsinger@berkeley.edu

Running title: KSHV ORF68 is essential for genome encapsidation

Abstract

Herpesviral DNA packaging into nascent capsids requires multiple conserved viral proteins that coordinate genome encapsidation. Here, we investigated the role of the ORF68 protein of Kaposi's sarcoma-associated herpesvirus (KSHV), a protein required for viral DNA encapsidation whose function remains largely unresolved across the herpesviridae. We found that KSHV ORF68 is expressed with early kinetics and localizes predominantly to viral replication compartments, although it is dispensable for viral DNA replication and gene expression. However, in agreement with its proposed role in viral DNA packaging, KSHV-infected cells lacking ORF68 failed to cleave viral DNA concatemers, accumulated exclusively immature B-capsids, and released no infectious progeny virions. ORF68 has no predicted domains aside from a series of putative zinc finger motifs. However, *in vitro* biochemical analyses of purified ORF68 protein revealed that it robustly binds DNA and is associated with nuclease activity.

24 These activities provide new insights into the role of KSHV ORF68 in viral genome
25 encapsidation.
26
27 **Importance**
28 Kaposi's sarcoma-associated herpesvirus (KSHV) is the etiologic agent of Kaposi's
29 sarcoma and several B-cell cancers, causing significant morbidity and mortality in
30 immunocompromised individuals. A critical step in the production of infectious viral progeny is
31 the packaging of the newly replicated viral DNA genome into the capsid, which involves
32 coordination between at least seven herpesviral proteins. While the majority of these
33 packaging factors have been well studied in related herpesviruses, the role of the KSHV ORF68
34 protein and its homologs remains unresolved. Here, using a KSHV mutant lacking ORF68, we
35 confirm its requirement for viral DNA processing and packaging in infected cells. Furthermore,
36 we show that the purified ORF68 protein directly binds DNA and is associated with a metal-
37 dependent cleavage activity on double stranded DNA *in vitro*. These activities suggest a novel
38 role for ORF68 in herpesviral genome processing and encapsidation.
39
40 **Introduction**
41 Herpesviruses are large, double-stranded DNA viruses with complex virion assembly and
42 maturation strategies. Following the expression of structural genes, capsids are assembled in
43 the nucleus, first through the production of fragile procapsids (1). Procapsids are formed by the
44 binding and orientation of capsid proteins onto a protein scaffold, which is subsequently
45 digested by the viral protease, forming the more stable B-capsids. B-capsids further mature

46 upon packaging of the viral genome, which displaces the digested scaffold proteins, resulting in
47 the mature C-capsid (2). In cases where DNA packaging fails, empty A-capsids lacking both
48 scaffolding proteins and the viral genome are produced (3).

49 The process of viral DNA replication generates head-to-tail concatemers, which are
50 cleaved into unit-length genomes as they are packaged into immature capsids. In alpha and
51 betaherpesviruses, DNA packaging is coordinated by seven viral proteins, each of which is
52 essential for both cleavage and packaging of the newly replicated genomes (2). The proteins
53 required for DNA packaging have been most extensively studied in the alphaherpesvirus Herpes
54 Simplex virus type 1 (HSV-1), where the essential proteins are UL6, UL15, UL17, UL25, UL28,
55 UL32, and UL33. UL6 forms a ring-shaped oligomer, which occupies one vertex of the
56 icosahedral capsid, forming the portal through which the DNA is threaded during both
57 packaging and unpackaging (4). UL28, UL15, and UL33 form the terminase motor, an ATP-
58 dependent motor that physically threads the viral genome through the portal complex into the
59 nascent capsid (5). Of the terminase motor, only UL28 has been shown to directly bind DNA (6).
60 However, UL15 and its homolog UL89 in betaherpesviruses have been shown to nick DNA
61 substrates *in vitro* (2, 7). UL17 and UL25 are part of the vertex-specific complex, which binds to
62 the vertices of the assembled capsid, as well as to the portal complex, thereby aiding docking of
63 the terminase motor (8, 9). UL32 is the only protein that is required for DNA cleavage and
64 packaging that lacks a well-defined function (2). However, UL32 contains a number of putative
65 C-X-X-C type zinc finger domains and mutation of these conserved motifs results in altered di-
66 sulfide patterns on the viral protease, which is involved in capsid assembly, supporting a role
67 for UL32 in viral genome encapsidation (10).

68 Significantly less is known about the DNA packaging process in gammaherpesviruses
69 such as Kaposi's sarcoma-associated herpesvirus (KSHV), although each of the packaging
70 proteins described above are conserved. These include KSHV ORF7 (UL28; terminase subunit),
71 ORF19 (UL25; vertex-specific complex), ORF29 (UL15; terminase subunit), ORF32 (UL17; vertex-
72 specific complex), ORF43 (UL6; portal protein), ORF67.5 (UL33; terminase subunit), and ORF68
73 (UL32; unknown). Cryo-electron microscopy of KSHV capsids indicated that KSHV ORF43 forms
74 the portal complex and that ORF32 is associated with vertices, consistent with studies in HSV-1
75 (11, 12).
76 Given that role ORF68 and its homologs play during viral DNA packaging are largely
77 unresolved across the herpesviridae, we sought to explore its function in more detail in KSHV-
78 infected cells and *in vitro*. During lytic KSHV infection, many features of ORF68 were conserved
79 with its alpha and betaherpesvirus homologs, such as localization to viral replication
80 compartments, and its requirement for viral genome cleavage, packaging, and infectious virion
81 production. Interestingly, biochemical analyses of recombinant ORF68 protein purified from
82 mammalian cells revealed it to be a robust DNA-binding protein that is associated with dsDNA
83 cleavage activity. These novel findings suggest that ORF68 plays a previously unappreciated role
84 in KSHV genome processing and encapsidation.
85
86 **Results**
87
88 **KSHV ORF68 is an early viral protein that localizes to viral replication compartments**

89 Although KSHV ORF68 has not been characterized, its homologs in alpha and
90 betaherpesviruses are expressed with late kinetics and are involved in viral DNA packaging (10,
91 13). ORF68 shares 24.8% sequence identity with UL32, its best characterized homolog from
92 HSV-1, including the five C-X-X-C motifs conserved across all the subfamily homologs (10). To
93 characterize the expression kinetics and potential functions of KSHV ORF68, we generated a
94 rabbit polyclonal antibody using recombinant ORF68 protein. We monitored the expression of
95 ORF68 in KSHV-infected iSLK.BAC16 cells, a commonly used Caki-1 cell line containing a
96 doxycycline (dox)-inducible version of the major viral lytic transactivator, ORF50 (RTA) (14, 15).
97 Lytic reactivation of these cells upon dox treatment revealed that ORF68 expression begins as
98 early as 6 hours post-reactivation and it is robustly expressed by 18 hours (Figure 1a). Its
99 expression kinetics mimicked those of the KSHV delayed early protein ORF59, and it was not
100 impacted by treatment with the viral DNA replication inhibitor phosphonoacetic acid (PAA),
101 which blocks expression of viral late genes such as K8.1 (Figure 1a). Thus, KSHV ORF68 is a
102 delayed early gene.

103 ORF68 has been alternatively annotated as a 467 amino acid (aa) protein and as a
104 longer, 545 aa protein containing a 78 aa N-terminal extension (ORF68-Extended) (Figure 1c).
105 However, on a western blot of iSLK.BAC16 lysate, ORF68 migrated as a single band at the
106 predicted molecular weight (MW) of the 467 aa form (52kDa). To confirm that the 467 aa
107 version was the expressed form in KSHV-infected cells, we cloned both versions into a
108 mammalian expression vector and compared their migration pattern in transfected HEK293T
109 cells to endogenous ORF68 in lytically-reactivated iSLK.BAC16 cells and the KSHV-infected B cell

110 line TREx-BCBL1. Indeed, in both cell lines, only the 467 aa form of ORF68 was detected (Figure
111 1b).

112 We next evaluated the subcellular localization of ORF68 in reactivated iSLK.BAC16 and
113 TREx-BCBL1 cells using immunofluorescence assays with the ORF68 antibody. To identify
114 infected cells, cells were co-stained with an antibody against the viral polymerase processivity
115 factor ORF59, which accumulates in viral replication compartments in the nucleus (16). We
116 observed no ORF68 staining in unreactivated or ORF59-negative cells, but in reactivated cells
117 ORF68 was present in both the cytoplasm and, more prominently, in the nucleus. In the
118 cytoplasm, it was primarily diffuse, but also localized to some randomly distributed puncta and
119 larger aggregates close to the nucleus. In the nucleus, ORF68 was localized predominantly in
120 viral replication compartments (Figure 2).

121

122 **KSHV lacking ORF68 maintains viral DNA replication and late gene expression, but does not**
123 **produce infectious virions**

124 To evaluate the role of ORF68 in the viral replication cycle, we generated an ORF68-
125 deficient virus (ORF68^{PTC}) using the BAC16 Red Recombinase system (14) by inserting two
126 premature termination codons 15 nt downstream of the translation start site. This virus was
127 used to establish a latently-infected cell line in iSLK cells. To ensure that any observed
128 phenotypes were not due to secondary mutations, we also engineered the corresponding
129 mutant rescue virus (ORF68^{PTC}-MR) (Figure 3a). Despite lacking ORF68 protein, the ORF68^{PTC}
130 virus expressed both the delayed early protein ORF59 and the late protein K8.1 at levels similar
131 to both the unmodified WT BAC16 KHSV and the ORF68^{PTC}-MR virus (Figure 3b). Furthermore,

132 qPCR analyses of viral DNA revealed no significant difference in DNA replication between any of
133 the viruses (Figure 3c). We then monitored production of infectious progeny virions using a
134 supernatant transfer assay, in which the supernatant from reactivated infected iSLK cells is
135 filtered and transferred to target cells. Because the BAC16-derived KSHV contains a virally-
136 encoded, constitutively-expressed GFP reporter gene, infected recipient cells can be quantified
137 by GFP expression using flow cytometry. Here, ORF68^{PTC} showed a marked defect, as no virus
138 production was detectable, while both WT and ORF68^{PTC}-MR infected cells produced sufficient
139 virus to infect nearly 100% of target cells (Figure 3d). Collectively, these data indicate that KSHV
140 ORF68 is essential for a late stage event in the viral replication cycle.
141
142 **In the absence of ORF68, KSHV DNA is not cleaved after replication**
143 The above results, together with studies of alpha and betaherpesvirus ORF68 homologs
144 (10, 13), suggested a role for KSHV ORF68 in viral DNA encapsidation. We therefore established
145 an assay similar to what has been used in other herpesviruses to measure packaging-associated
146 KSHV DNA cleavage, which occurs within the 801 bp GC-rich terminal repeat (TR) sequences
147 present in 20 – 40 tandem copies in the KSHV genome (17) (Figure 4a). Briefly, DNA was
148 isolated from infected iSLK cells and the TR sequences were released by digesting the DNA with
149 PstI-HF, which cleaves frequently within viral (and host) DNA, but not within the KSHV TRs. This
150 should generate a ladder of TR sequences, representing the collection of individual cleavage
151 events in the TRs that occur during packaging, which can be visualized by Southern blotting
152 with a DIG-labeled TR probe. As expected, we observed a robust increase in the high MW
153 uncleaved TRs following lytic reactivation of each sample, indicative of viral genome replication

154 (Figure 4b). However, DNA from ORF68^{PTC} infected cells showed no evidence of TR cleavage,
155 unlike DNA from WT and ORF68^{PTC}-MR infected cells, which displayed the expected laddering
156 phenotype (Figure 4b).
157
158 **KSHV ORF68^{PTC} cannot progress past the B-capsid stage of virion assembly**
159 During herpesvirus assembly, immature B-capsids are initially formed that contain
160 internal scaffolding proteins, which are subsequently proteolytically cleaved and extruded
161 during the process of DNA packaging (18, 19). This yields either mature, DNA-containing C-
162 capsids, or, in the case of unsuccessful DNA packaging, empty A-capsids (20). To visualize the
163 contribution of ORF68 towards capsid maturation, we performed transmission electron
164 microscopy on fixed samples of lytically-reactivated iSLK cells containing either WT or ORF68^{PTC}
165 KSHV. In the nuclei of WT KSHV infected cells, we observed A, B, and C capsids (Figure 5a, b). In
166 contrast, ORF68^{PTC} infected cells contained exclusively B capsids (Figure 5a, b), indicating that
167 KSHV DNA packaging is not initiated in the absence of ORF68.
168
169 **ORF68 binds DNA with high affinity *in vitro* and is associated with metal-dependent nuclease**
170 **activity**
171 In order to study the biochemical activity of ORF68 as it relates to DNA packaging, we
172 sought to generate pure ORF68 protein. Our attempts to isolate recombinant ORF68 from *E.*
173 *coli* bacteria, *Pichia pastoris* yeast, and *SF9* insect cells did not yield properly folded protein
174 (data not shown). Thus, we instead purified TwinStrep-tagged ORF68 from transiently
175 transfected HEK293T cells by binding to Strep-TactinXT resin, followed by separation of ORF68

176 from the TwinStrep tag by PreScission protease cleavage and subsequent size exclusion
177 chromatography (Figure 6a). Mass spectrometry of the purified sample detected ORF68 but no
178 other contaminating proteins (data not shown). Notably, ORF68 eluted from gel filtration
179 columns as a ~275 kDa oligomer (based on injected standards) rather than as a monomer
180 (Figure 6b).

181 Given the failed DNA cleavage and packaging phenotypes associated with the ORF68^{PTC}
182 virus, we hypothesized that ORF68 might directly bind the viral genome to help direct DNA
183 packaging. We therefore used electrophoretic mobility shift assays (EMSA) to monitor binding
184 of purified ORF68 to a DNA probe containing the sequence of the KSHV TR *in vitro*. Indeed,
185 ORF68 efficiently bound DNA with an apparent K_d of (53.34 ± 2.11) nM (Figure 7a, b). The
186 binding was cooperative, with a Hill coefficient of 1.88 ± 0.12 (Figure 7b). This is comparable to
187 the 72 nM K_d of KSHV LANA binding to the terminal repeat (21). Multiple higher-order binding
188 events occurred at increased protein concentrations, resulting in several discrete bands of
189 protein-bound DNA (Figure 7a). Although this *in vitro* DNA-binding is robust, it does not appear
190 to be specific, as similar length probes of varying GC content from disparate sources were
191 bound with similar affinity (data not shown).

192 ORF68 has no identifiable domains aside from several predicted zinc finger motifs that
193 appear to be important for the structural integrity of the protein (22). However, we noted that
194 in the presence of Mg^{2+}, the TR probe or other plasmid DNA was degraded upon incubation
195 with ORF68, suggesting that it may possess nuclease activity (Figure 7c, data not shown).
196 Nuclease activity required metal ions for catalysis, with a preference for Mg^{2+} or Mn^{2+},
197 drastically reduced activity with Co^{2+} or Ni^{2+}, and no activity with Ca^{2+} or Zn^{2+} (Figure 7d).

198 Reactions were sensitive to EDTA or similar metal-chelating agents, consistent with our
199 observations that EDTA-containing buffers caused the precipitation of ORF68. Although our
200 mass spectrometry analysis of purified ORF68 did not detect contaminating peptides, at
201 present we cannot formally rule out the possibility that trace levels of a cellular nuclease co-
202 purified with ORF68, rather than nuclease activity being an intrinsic feature of ORF68. However,
203 given that ORF68 contains putative zinc finger motifs, we reasoned that in addition to inhibition
204 by EDTA, the associated nuclease activity should be sensitive to the zinc-specific chelator
205 N,N,N′,N′-tetrakis(2-pyridinylmethyl)-1,2-ethanediamine (TPEN), which has high affinity for Zn^{2+}
206 (K_d= 2.6 x 10^{-16} M), but very low affinity for Mg^{2+} (K_d= 2.6 x 10^{-2} M) and other divalent cations
207 (23-25). Indeed, the addition of TPEN prevented degradation of DNA in the presence of ORF68,
208 but not DNase I, a nuclease that requires Mg^{2+} for catalysis but does not contain any structural
209 zinc (Figure 7e). Collectively, these data demonstrate that KSHV ORF68 is a zinc finger-
210 containing protein that can bind DNA and is associated with a zinc-dependent DNase activity.
211
212 **Discussion**
213
214 Our data firmly establish that KSHV ORF68 is essential for genome encapsidation in
215 infected cells, and further suggest novel roles for purified ORF68 protein in DNA binding and
216 cleavage. This is the first demonstration of direct DNA binding by a DNA packaging-associated
217 protein in gammaherpesviruses, and the ORF68-associated nuclease activity suggests a
218 previously unappreciated function for this protein, which may relate to viral genome processing
219 and encapsidation. Such a role would be consistent with the defects in viral TR cleavage, DNA

220 packaging, and infectious virion formation we observed in cells infected with the ORF68^{PTC}
221 virus. It is further supported by our TEM analysis of infected cells, which showed that in the
222 absence of ORF68, DNA encapsidation was not initiated, as evidenced by the absence of A- and
223 C-capsids. Finally, our data are in line with phenotypes observed upon deletion of the ORF68
224 homologs in HSV-1 (10), HCMV (13) and Epstein-Barr virus (EBV) (26). Indeed, in EBV, deletion
225 of this BFLF1 gene was used to generate defective viral particles for use in vaccine development
226 (26).

227 The ORF68 homolog in HSV-1 (UL32) was recently shown to be involved in modulation of
228 disulfide bond formation during procapsid formation, which requires the presence of the
229 conserved C-X-X-C motifs (10). Deletion of individual cysteines within four of the five motifs
230 prevented complementation of a UL32 deletion mutant virus, and in the absence of UL32 the
231 disulfide bond profiles of other viral proteins were altered. In ORF68, however, the C-X-X-C
232 motifs appear to be important for its structural integrity, as chelation of Zn^{2+} causes ORF68 to
233 precipitate during purification in a manner that suggests unfolding (unpublished observations).
234 Thus, an important future challenge will be to resolve if these two functions are related, or if
235 specific roles for UL32 and ORF68 have diverged between the alpha- and gammaherpesviruses.

236 In the KSHV episome, the terminal repeats are present as 20 to 40 copies of a highly
237 repetitive ~800bp, 85% GC sequence (27). Unlike related herpesviruses, the packaging and
238 cleavage signals in the KSHV terminal repeats are unknown. However, by using a probe
239 generated from the entire repeat we could capture terminal repeats of any length. In a WT
240 KSHV infection, this yields a ladder-like cleavage pattern reflective of the fact that the genome
241 is replicated as head-to-tail concatemers, separated by an arbitrary number of terminal repeats.

242 While each genome should be cut only once at each end during packaging, the specific number
243 of repeats left at each genome terminus is variable (28, 29). This is in contrast to viruses lacking
244 ORF68, which displayed WT levels of DNA replication by both qPCR and Southern blotting, but
245 no apparent resolution of the amplified concatemers into unit-length genomes. These data
246 reinforce the hypothesis that KSHV ORF68 is not required for genome replication but is integral
247 to the process of DNA encapsidation.

248 Given the stage at which ORF68^{PTC} virus fails during virion maturation, we hypothesized
249 that ORF68 may interact with the viral genome to promote DNA packaging. Indeed, purified
250 ORF68 robustly bound the prototypical terminal repeat subunit, with an observed K_d of ~50nM.
251 This is comparable to the strength of the TR interaction for the KSHV latency-associated
252 episome tethering protein LANA, strongly suggesting that viral DNA binding is a biologically
253 relevant feature of ORF68 (21). However, it is important to note that *in vitro*, the DNA binding
254 activity of ORF68 does not have apparent sequence specificity. In cells, it is possible that
255 sequence specificity is conferred by other viral (or cellular) factors. Alternatively, given that
256 host DNA is largely excluded from replication compartments, sequence specific DNA binding
257 may not be required. It is also possible that the DNA binding activity participates in a distinct
258 facet of the viral lifecycle, although we did not detect any defects in the ORF68^{PTC} virus prior to
259 encapsidation. The ~800bp terminal repeat subunits are somewhat long for traditional EMSA
260 probes and as such, multiple binding events could be observed. Furthermore, binding of ORF68
261 to DNA was cooperative, as is frequently observed for DNA binding proteins (30). This
262 cooperativity may indicate that ORF68 binds the DNA probe at multiple sites, that the binding

263 of the first ORF68 molecule alters the DNA conformation in a way that promotes additional
264 ORF68 binding, or simply reflect our observation that ORF68 exists as an oligomer in solution.

265 In addition to DNA binding, we made the unexpected observation that in the presence
266 of the divalent cations Mg^{2+} or Mn^{2+}, incubation with ORF68 caused degradation of DNA. These
267 cations are commonly used by nucleases (31), and future studies are aimed at exploring
268 residues in ORF68 that could serve to coordinate divalent cations. Our robust purification
269 scheme, coupled with the absence of any detectable co-purifying peptides by mass
270 spectrometry and the fact that addition of the zinc-chelator TPEN specifically blocked ORF68-
271 associated nuclease activity suggest that the activity is intrinsic to ORF68. However, aside from
272 the zinc finger motifs, no predicted domains or structural information is currently available for
273 ORF68. Thus, a key challenge will be to establish if and how ORF68 promotes DNA cleavage in
274 cells. Formal proof of nuclease activity will ultimately require structural data to identify putative
275 catalytic domain(s), which should enable isolation of point mutants to be tested for DNA
276 cleavage. Similar to the DNA binding activity, our *in vitro* cleavage reactions do not capture TR-
277 specific targeting, as we found that other non-viral DNA was similarly susceptible to ORF68-
278 associated degradation (unpublished observations). This might suggest that other components
279 of the packaging machinery are required to confer specificity or, alternatively, that the putative
280 nuclease activity is involved in an ORF68 function independent of DNA encapsidation.

281 While seven herpesviral proteins are required for proper DNA encapsidation, only two
282 have been shown to directly act on DNA. A crystal structure of a fragment of the HSV-1 UL15
283 terminase motor protein, which is homologous to KSHV ORF29, revealed that it adopts an
284 RNase H-like fold and possess non-specific DNA nicking *in vitro* (7, 32). Purified HSV-1 UL28,

285 another terminase motor protein and the homolog of KSHV ORF7, has also been shown to bind
286 terminal repeat DNA *in vitro* (6). It has high specificity for certain terminal repeat DNA probes,
287 but only after heat treatment of the DNA, which causes them to adopt non-duplex structures
288 (6). This suggests that the UL28-DNA interaction is structure dependent, in contrast to KSHV
289 ORF68, which bound duplex DNA with no apparent sequence specificity or requirement for
290 higher order structures. Whether the UL15 and UL28 functions are conserved in their KSHV
291 homologs ORF29 and ORF7, and how KSHV ORF68 mechanistically contributes to DNA
292 encapsidation remain to be established.

293 Finally, although the majority of ORF68 is concentrated in replication compartments, the
294 protein also localizes within discrete puncta in the cytoplasm, as well as in larger aggregates
295 adjacent to the nucleus. While we hypothesize that the larger structures represent unfolded
296 protein in aggresomes, the smaller punctate structures are suggestive of a distinct function for
297 ORF68 in the cytoplasm, possibly unrelated to its role in packaging. Notably, HSV-1 UL32 was
298 also shown to localize to the cytoplasm, particularly late in infection, where it forms perinuclear
299 foci (10). Given the frequently multifunctional roles of viral proteins, it will be of interest to
300 explore possible additional cytoplasmic activities of ORF68.

301

302 **Methods**

303

304 **Plasmids**

305 TwinStrep-PreScission-ORF68 was cloned into the pHEK293 UltraExpression I vector
306 (Clontech) digested with XhoI and SalI. ORF68 was amplified with the primers 5'-

307 TGGAATTCTGCAGATATGTTTGTTCCCTGGCAACTCG-3' and 5'-
308 GCCACTGTGCTGGATTCAAGCGTACAAGTGTGACGTCT-3' while TwinStrep-PreScission was
309 amplified using the primers 5'-
310 CCTCCCCGGGCTCGAATGAGTGCGTGGAGTCATCCTCAATTCGAGAAAGGTG-3' and 5'-
311 GGGCCCCTGGAACAGAACTTCCAGTCCGGATTTTTCGAACTGCGGG-3'. The two fragments were
312 first assembled by PCR and then inserted into the vector by InFusion cloning (Clontech).
313 ORF68 and ORF68-Extended were cloned into pCDNA4 (ThermoFisher) digested with
314 EcoRV using 5'-TGGAATTCTGCAGATATGTTTGTTCCCTGGCAACTCG-3' for ORF68, 5'-
315 TGGAATTCTGCAGATATGTCACGAGGCAGAAGCTGG-3' for ORF68-Extended, and 5'-
316 GCCACTGTGCTGGATTCAAGCGTACAAGTGTGACGTCT-3' as the reverse primer for both. PCR
317 products were inserted into the vector using InFusion cloning.
318
319 **Cell Lines**
320 HEK293T (ATCC CRL-3216) cells were maintained in DMEM +10% FBS. HEK293T-ORF68
321 cells were maintained in DMEM + 10% FBS, 325 µg/ml zeocin. iSLK.BAC16 (14) cells were
322 maintained in DMEM + 10% FBS, 1 mg/ml hygromycin B, and 1 µg/ml puromycin. TREx-BCBL1
323 (33) cells were maintained in RPMI 1640 + 20% FBS.
324
325 **Viral mutagenesis and infection studies**
326 The KSHV ORF68 Premature Termination Codon (ORF68^{PTC}) mutant and corresponding
327 mutant rescue (MR) were engineered using the scarless Red recombination system in BAC16
328 GS1783 *E. coli* as previously described (14), except using two gBlocks (IDT) to introduce the

329 mutation. Each gBlock contained half of the kanamycin resistance cassette, as well as the
330 desired mutation, and were joined by short overlap extension PCR before being used as the
331 linear insert in the established protocol.

332 The BAC16 ORF68 mutant and MR were purified using the NucleoBond BAC 100 kit
333 (Clontech). iSLK cell lines latently infected with the KSHV ORF68^{PTC} virus were then established
334 by co-culture of the relevant BAC16-containing HEK293T cells with uninfected target iSLK-Puro
335 cells. HEK293T cells constitutively expressing ORF68 (HEK293T-ORF68) were transfected with 12
336 µg of BAC16 containing ORF68^{PTC} or MR using linear polyethylenimine (PEI, MW ~25,000) at a
337 1:3 DNA:PEI ratio. The following day, the cells were trypsinized and mixed 1:1 with iSLK-puro
338 cells, then treated with 30 nM 12-O-Tetradecanoylphorbol-13-acetate (TPA) and 300 nM
339 sodium butyrate for 4 days to induce lytic replication. Cells were then incubated with selection
340 media containing 300 µg/ml hygromycin B, 1 µg/ml puromycin, and 250 µg/ml G418. Media
341 was replaced every other day for ~2 weeks, gradually increasing the hygromycin B
342 concentration to 1 mg/ml until there were no HEK293T cells remaining and the iSLK cells were
343 green and replicating.

344 For induction studies, BAC16-containing iSLK cells were treated with 1 µg/ml doxycycline
345 and 1 mM sodium butyrate, and TREx-BCBL1 cells were induced with doxycycline (1 ug/ml) and
346 TPA (25 ng/ml) for the indicated amount of time. Virion production from reactivated iSLK cells
347 was measured using supernatant transfer assays at 72 hours post induction. The supernatant
348 was filtered through a 0.45 µM PES filter, then 2 ml were mixed with $1x10^6$ freshly trypsinized
349 HEK293T cells. The cell mixture was placed into a 6 well plate and centrifuged at 1,200 x *g* for 2
350 hours at 32˚C. The following day, cells were trypsinized, fixed in 4% paraformaldehyde, then

351 analyzed for GFP expression by flow cytometry (BD Csampler, BD Biosciences). Data was
352 analyzed using FlowJo v10.
353
354 **Generation of HEK293T cells stably expressing ORF68**
355 HEK293T-ORF68 cells were generated by cloning ORF68 into pLJM1 (a gift from David
356 Sabatini (Addgene plasmid #19319) (34)) in which the puromycin resistance had been
357 exchanged for zeocin. The vector was digested with AgeI and EcoRI (New England Biolabs) and
358 ORF68 was amplified by PCR using primers 5'-
359 CGCTAGCGCTACCGGATGTTTGTTCCCTGGCAACTCGG-3' and 5'-
360 TCGAGGTCGAGAATTTCAAGCGTACAAGTGTGACGTCTG-3' and inserted using T4 DNA Ligase
361 (NEB). 1.6 µg of this plasmid was co-transfected into HEK293T cells along with the lentiviral
362 packaging plasmids pMD2.G (0.5 µg) and psPAX2 (1.3 µg) (gifts from Didier Trono (Addgene
363 plasmid #12259 and #12260)) using PEI. 48 hours after transfection, the supernatants were
364 collected, filtered through a 0.45 µm PES filter, diluted 1:4 (supernatant:media) in serum-free
365 DMEM containing 8 µg/ml of polybrene, and added to the wells of a 6 well plate containing
366 $1x10^6$ HEK293T cells per well. The plates were centrifuged for 2 hours at 1,200 x *g* (32˚C),
367 incubated overnight, and the media replaced with fresh DMEM (10% FBS) containing 325 µg/ml
368 zeocin until no further cell death was observed, roughly two weeks.
369
370 **Western blots and antibody production**
371 Cells were lysed in protein lysis buffer (50 mM Tris-HCl pH 7.6, 150 mM NaCl, 3 mM
372 $MgCl_2$, 10% glycerol, 0.5% NP-40, cOmplete EDTA-free Protease Inhibitors [Roche]) and clarified

373 by centrifugation at 20,000 x *g* for 10 min at 4˚C. Lysates were resolved by SDS-PAGE and
374 western blotted with rabbit anti-ORF68 (1:5000), rabbit anti-ORF59 (1:10,000), rabbit anti-K8.1
375 (1:10,000), rabbit anti-histone H3 (1:3000, Cell Signaling 4499S), or mouse anti-GAPDH (1:5000,
376 Abcam ab8245). Rabbit anti-ORF68, -ORF59, and -K8.1 was produced by Pocono Rabbit Farm &
377 Laboratory by immunizing rabbits against MBP-ORF68, -ORF59, or -K8.1 (gifts of Denise Whitby,
378 (35)). Sera was harvested and used directly for ORF59 and K8.1, while ORF68-specific antibodies
379 were isolated by first collecting antibodies that bound an MBP-ORF68 column, followed by
380 removal of non-specific antibodies on an MBP column. Both selection columns were generated
381 using the AminoLink Plus Immobilization Kit (ThermoFisher).
382
383 **Immunofluorescence assays**
384 Cells were fixed with 4% paraformaldehyde, permeabilized with ice-cold methanol at -
385 20˚C for 20 min, then blocked with BSA blocking buffer (PBS, 1% Triton X-100, 0.5% Tween20,
386 3% BSA) for 30 minutes at room temperature. They were then incubated with rabbit anti-ORF68
387 and mouse anti-ORF59 (Advanced Biotechnologies) antibodies (diluted 1:100 in blocking buffer)
388 overnight at 4˚C, washed with PBS, and incubated with secondary antibody (AlexaFluor594 or
389 DyLight650, 1:1000 in BSA blocking buffer) for 1 h at 37˚C, and mounted using VectaShield
390 HardSet with DAPI (ThermoFisher). Images were acquired on an EVOS FL inverted fluorescent
391 microscope (ThermoFisher).
392
393 **DNA isolation and qPCR**

394 iSLK-BAC16 cells were incubated with 5x proteinase K digestion buffer (50 mM Tris-HCl
395 pH 7.4, 500 mM NaCl, 5 mM EDTA, 2.5% SDS) and digested with proteinase K (80 µg/ml)
396 overnight at 55˚C. The gDNA was isolated using Zymo Quick gDNA Miniprep Kit according to the
397 manufacturer's instructions.

398 Quantitative PCR was performed on the isolated DNA using iTaq Universal SYBR Green
399 Supermix on a QuantStudio3 Real-Time PCR machine. DNA levels were quantified using relative
400 standard curves with primers specific for KSHV ORF57 (5'-GGTGTGTCTGACGCCGTAAAG-3' and
401 5'-CCTGTCCGTAAACACCTCCG-3') or a region in the GAPDH promoter (5'-
402 TACTAGCGGTTTTACGGGCG-3' and 5'-TCGAACAGGAGGAGCAGAGAGCGA-3'). The relative
403 genome numbers were normalized to GAPDH to account for loading differences and to
404 uninduced samples to account for starting genome copy number.

405

406 **Protein purification**

407 TwinStrep-PreScission-ORF68 was transfected using PEI into 50 90% confluent 15 cm
408 plates of HEK293T cells for 48h. Cells were lysed in 5 ml of lysis buffer (100 mM Tris-HCl pH 8.0,
409 300 mM NaCl, 1 mM DTT, 5% glycerol, 0.1% CHAPS, 1 µg/ml avidin, cOmplete EDTA-free
410 protease inhibitors [Sigma-Aldrich]) per 1 g of cell pellet and rotated at 4˚C for an additional 30
411 minutes. The viscosity was reduced by sonication, whereupon debris was removed by
412 centrifugation at 20,000 x *g* (4˚C) for 30 min followed by filtration through a 0.45 µm PES filter
413 with a glass pre-filter (Millipore). Lysate was passed three times over a gravity column
414 containing Strep-Tactin XT Superflow slurry (IBA) then washed with 5 column volumes of strep
415 running buffer (100 mM Tris-HCl pH 8.0, 300 mM NaCl, 1 mM DTT, 5% glycerol, 0.1% CHAPS).

416 ORF68 was eluted by rotating the column overnight in HRV 3C Protease (Millipore) at a 1:100
417 Protease:ORF68 ratio in buffer containing 2 mM DTT, then concentrated to ~500 µL using a 30
418 kDa cut-off Centriprep spin concentrator (Millipore). The concentrated eluate was centrifuged
419 at 20,000 x *g* for 10 min to remove precipitates and injected onto a HiLoad 16/600 Superdex
420 200 pg gel filtration column (GE Healthcare), previously equilibrated with Gel Filtration buffer
421 (50 mM HEPES pH 7.6, 100 mM NaCl, 100 mM KCl, 5% glycerol, 0.1% CHAPS). Gel filtration was
422 performed using an AKTA Pure FPLC (GE Healthcare). Fractions resulting from the gel filtration
423 were analyzed by SDS-PAGE and staining with colloidal Coomassie (36). Fractions containing
424 ORF68 were pooled and concentrated as before, until the total concentration was ~2 mg/mL as
425 evaluated by absorbance at 280 nm. The concentrated protein was injected into a 20 kDa cut-
426 off Slide-A-Lyzer dialysis cassette (ThermoFisher) and dialyzed against storage buffer (Gel
427 Filtration buffer lacking CHAPS). Dialyzed protein was diluted to 1 mg/ml, aliquoted, and snap-
428 frozen in liquid nitrogen before being stored at -80˚C.
429
430 **Electrophoretic mobility shift assay**
431 Single-subunit terminal repeat DNA probes were generated by digesting pK8TR (a gift of
432 the Kaye lab (17)) with AscI overnight. The resulting cleavage products were separated on an
433 agarose gel and the 800bp band was excised, isolated from agarose, and purified further by
434 phenol:chloroform extraction and ethanol precipitation.
435 EMSA assays were assembled on ice in gel shift buffer (25 mM HEPES pH 7.6, 50 mM
436 NaCl, 50 mM KCl, 0.1 mg/ml BSA, 0.05% CHAPS, 10% glycerol) with 5 nM probe and 2-fold
437 dilutions of ORF68 ranging from 1.95 nM to 1000 nM. Once assembled, the reactions were

438 incubated at 30˚C for 30 minutes. Samples were directly loaded onto a 3.5% 29:1
439 polyacrylamide:bisacrylamide native gel containing 45 mM Tris-borate pH 8.3, 10% glycerol,
440 which was degassed thoroughly before polymerization. Samples were separated by
441 electrophoresis at 250V for 1 hour at 4˚C in pre-chilled 0.5X TB (45 mM Tris-borate pH 8.3). Tris-
442 borate buffer was used in lieu of TBE because ORF68 precipitates in the presence of EDTA. The
443 native polyacrylamide gel was cast to a final concentration of 0.5X Tris-borate, 10% glycerol,
444 and was degassed thoroughly before polymerization. Following the electrophoresis, the gel was
445 removed from the running cassette and stained with SYBRgold (ThermoFisher) in 0.5X TB for 30
446 minutes, rocking at room temperature and protected from light. Staining solution was removed
447 by briefly washing with fresh 0.5X TB and the gel was imaged on a ChemiDoc Touch (Bio-rad).
448 All bands were quantified using ImageLab v6.0 (Bio-rad) and percent bound probe was
449 determined by dividing shifted band intensity by the total intensity of all bands in that lane.
450 Binding curves were generated using Prism v7 (GraphPad) by non-linear regression fit using
451 least-squares. Shown data represents three technical replicates performed on different days.
452
453 **Nuclease assays**
454 The EMSA probe was also used for nuclease assays and was produced as described
455 above. Reactions were assembled in nuclease buffer (25 mM HEPES pH 7.6, 50 mM NaCl, 50
456 mM KCl, 0.1 mg/ml BSA, 2.5 mM $MgCl_2$) with 1 nM DNA probe and 2-fold dilutions of ORF68
457 ranging from 9.77 to 5000 nM. The reactions were incubated at 37˚C overnight. The following
458 day, reactions were quenched using stop buffer (4 M urea, 50 mM EDTA, 1 mM $CaCl_2$, 0.8 U
459 proteinase K [New England Biolabs], 1x Purple Loading dye [New England Biolabs]; final

460 concentrations) and incubating at room temperature for 30 minutes. The samples were then
461 loaded onto a denaturing polyacrylamide gel (8 M Urea, 4.5% 29:1 acrylamide:bisacrylamide,
462 90 mM Tris-borate pH 8.3, 2 mM EDTA, degassed before polymerization), which had been pre-
463 run at 200V for 30 minutes in 1X TBE to evenly heat the gel. The samples were separated at
464 200V for 45 minutes before being removed from the running cassette and stained with
465 SYBRgold in 1X TBE for 30 minutes at room temperature, protected from light. Gels were
466 visualized using a ChemiDoc Touch (Bio-Rad). Metal-dependence tests were performed as
467 described but changing the 2.5 mM $MgCl_2$ to the chloride salts of the indicated divalent cations.
468 TPEN-treatment was performed as described but protein was treated with either TPEN in 100%
469 ethanol (1 mM), mock treated with 100% ethanol, or EDTA (50 mM) for 10 minutes on ice prior
470 to adding the DNA substrate. DNaseI (New England Biolabs) was diluted to 0.02U in ORF68
471 storage buffer before addition to reactions.
472
473 **Southern blotting**
474 BAC16.iSLK cells were harvested in proteinase K digestion buffer and incubated
475 overnight with proteinase K (80 µg/ml). DNA was isolated by phenol:chloroform extraction and
476 ethanol precipitation, then resuspended in TE buffer. DNA (10 µg) was digested with PstI-HF
477 (New England Biolabs) overnight then separated by electrophoresis in a 0.7% agarose 1x TBE
478 gel stained with SYBRsafe. The DNA was transferred to a NYTRAN-N membrane (GE Healthcare)
479 by capillary action in 20x SSC overnight and crosslinked to the membrane in a StrataLinker 2400
480 (Stratagene) using the AutoUV setting.

481 The membrane was treated according to the DIG High Prime DNA Labeling and
482 Detection Starter Kit II (Roche) following the manufacturer's instructions. Briefly, the
483 membrane was hybridized at 42˚C in EasyHyb Buffer with a DIG-labeled linear terminal repeat
484 subunit derived from AscI (New England Biolabs) digested pK8TR, which was labeled according
485 to kit instructions. Following overnight hybridization, the membrane was washed twice with 2X
486 SSC (+0.1% SDS) at room temperature and then twice with 0.5X SSC (+0.1% SDS) at 68˚C. Using
487 supplied reagents, the blot was then blocked, incubated with anti-DIG-AP antibody, and
488 visualized on a ChemiDoc Touch (Bio-Rad).
489
490 **Electron microscopy**
491 iSLK.BAC16 WT or ORF68^{PTC}-infected cells were induced for 48 hours as described
492 above. Cells were washed once with PBS and fixed with 2% glutaraldehyde, 4%
493 paraformaldehyde in 100 mM sodium cacodylate buffer, pH 7.2 for 10 minutes at room
494 temperature. Fixative was removed and cells were scraped into 2% glutaraldehyde in 100 mM
495 sodium cacodylate buffer, pH 7.2 and evenly resuspended by pipetting. Cells were then washed
496 with 1% osmium tetroxide, 0.8% ferricyanide in 100 mM sodium cacodylate buffer, pH 7.2,
497 before being treated with 1% uranyl acetate and dehydrated with increasing concentrations of
498 acetone. Samples were then infiltrated and embedded in resin, from which 70 nm sections
499 were cut on a Reichert-Jung microtome. Sections were picked up on copper mesh grids coated
500 with 0.5% formvar, post-stained with uranyl acetate and lead citrate, and examined using an FEI
501 Tecnai 12 transmission electron microscope.
502

Acknowledgements

We thank all members of the Glaunsinger and Coscoy labs, in particular Angelica Castañeda and Allison Didychuk, as well as Dr. Sandra Weller for their helpful suggestions and critical reading of the manuscript. We also thank Reena Zalpuri and all of the staff at the University of California Berkeley Electron Microscope Laboratory for advice and assistance in electron microscopy sample preparation and data collection. B.G. is an investigator of the Howard Hughes Medical Institute. This research was also supported by NIH R01AI122528 to B.G.

512 **References**

513 1. **Rixon FJ**, **McNab D**. 1999. Packaging-competent capsids of a herpes simplex virus
514 temperature-sensitive mutant have properties similar to those of in vitro-assembled
515 procapsids. J Virol **73**:5714–5721.

516 2. **Heming JD**, **Conway JF**, **Homa FL**. 2017. Herpesvirus Capsid Assembly and DNA Packaging,
517 pp. 119–142. *In* Cell Biology of Herpes Viruses, 5 ed. Springer International Publishing,
518 Cham.

519 3. **Booy FP**, **Newcomb WW**, **Trus BL**, **Brown JC**, **Baker TS**, **Steven AC**. 1991. Liquid-crystalline,
520 phage-like packing of encapsidated DNA in herpes simplex virus. Cell **64**:1007–1015.

521 4. **Cardone G**, **Winkler DC**, **Trus BL**, **Cheng N**, **Heuser JE**, **Newcomb WW**, **Brown JC**, **Steven AC**.
522 2007. Visualization of the herpes simplex virus portal in situ by cryo-electron tomography
523 **361**:426–434.

524 5. **Heming JD**, **Huffman JB**, **Jones LM**, **Homa FL**. 2013. Isolation and Characterization of the
525 Herpes Simplex Virus 1 Terminase Complex. J Virol **88**:225–236.

526 6. **Adelman K**, **Salmon B**, **Baines JD**. 2001. Herpes simplex virus DNA packaging sequences
527 adopt novel structures that are specifically recognized by a component of the cleavage and
528 packaging machinery. Proc Natl Acad Sci USA **98**:3086–3091.

529 7. **Selvarajan Sigamani S**, **Zhao H**, **Kamau YN**, **Baines JD**, **Tang L**. 2013. The Structure of the
530 Herpes Simplex Virus DNA-Packaging Terminase pUL15 Nuclease Domain Suggests an
531 Evolutionary Lineage among Eukaryotic and Prokaryotic Viruses. J Virol **87**:7140–7148.

532 8. **Thurlow JK**, **Murphy M**, **Stow ND**, **Preston VG**. 2006. Herpes Simplex Virus Type 1 DNA-
533 Packaging Protein UL17 Is Required for Efficient Binding of UL25 to Capsids. J Virol **80**:2118–
534 2126.

535 9. **Newcomb WW**, **Homa FL**, **Brown JC**. 2006. Herpes Simplex Virus Capsid Structure: DNA
536 Packaging Protein UL25 Is Located on the External Surface of the Capsid near the Vertices. J
537 Virol **80**:6286–6294.

538 10. **Albright BS**, **Kosinski A**, **Szczepaniak R**, **Cook EA**, **Stow ND**, **Conway JF**, **Weller SK**. 2014. The
539 Putative Herpes Simplex Virus 1 Chaperone Protein UL32 Modulates Disulfide Bond
540 Formation during Infection **89**:443–453.

541 11. **Deng B**, **O'Connor CM**, **Kedes DH**, **Zhou ZH**. 2008. Cryo-electron tomography of Kaposi's
542 sarcoma-associated herpesvirus capsids reveals dynamic scaffolding structures essential to
543 capsid assembly and maturation. Journal of Structural Biology **161**:419–427.

544 12. **Dai X**, **Gong D**, **Wu TT**, **Sun R**, **Zhou ZH**. 2014. Organization of Capsid-Associated Tegument
545 Components in Kaposi's Sarcoma-Associated Herpesvirus. J Virol **88**:12694–12702.

546 13. **Borst EM**, **Wagner K**, **Binz A**, **Sodeik B**, **Messerle M**. 2008. The Essential Human
547 Cytomegalovirus Gene UL52 Is Required for Cleavage-Packaging of the Viral Genome
548 **82**:2065–2078.

549 14. **Brulois KF**, **Chang H**, **Lee AS-Y**, **Ensser A**, **Wong L-Y**, **Toth Z**, **Lee SH**, **Lee H-R**, **Myoung J**,
550 **Ganem D**, **Oh T-K**, **Kim JF**, **Gao S-J**, **Jung JU**. 2012. Construction and Manipulation of a New
551 Kaposi's Sarcoma-Associated Herpesvirus Bacterial Artificial Chromosome Clone. J Virol
552 **86**:9708–9720.

553 15. **Myoung J**, **Ganem D**. 2011. Generation of a doxycycline-inducible KSHV producer cell line of
554 endothelial origin: Maintenance of tight latency with efficient reactivation upon induction.
555 Journal of Virological Methods **174**:12–21.

556 16. **Wu FY**, **Ahn JH**, **Alcendor DJ**, **Jang WJ**, **Xiao J**, **Hayward SD**, **Hayward GS**. 2001. Origin-
557 Independent Assembly of Kaposi's Sarcoma-Associated Herpesvirus DNA Replication
558 Compartments in Transient Cotransfection Assays and Association with the ORF-K8 Protein
559 and Cellular PML. J Virol **75**:1487–1506.

560 17. **Habison AC**, **de Miranda MP**, **Beauchemin C**, **Tan M**, **Cerqueira SA**, **Correia B**, **Ponnusamy**
561 **R**, **Usherwood EJ**, **McVey CE**, **Simas JP**, **Kaye KM**. 2017. Cross-species conservation of
562 episome maintenance provides a basis for in vivo investigation of Kaposi's sarcoma
563 herpesvirus LANA. PLoS Pathog **13**:e1006555–25.

564 18. **Gibson W**, **virology BRJO**, **1972**. Proteins specified by herpes simplex virus VIII.
565 Characterization and composition of multiple capsid forms of subtypes 1 and 2. Am Soc
566 Microbiol.

567 19. **Rixon FJ**, **Cross AM**, **Addison C**, **Preston VG**. 1988. The products of herpes simplex virus type
568 1 gene UL26 which are involved in DNA packaging are strongly associated with empty but
569 not with full capsids. Journal of General Virology **69 (Pt 11)**:2879–2891.

570 20. **Tandon R**, **Mocarski E**, **Conway J**. 2015. The A, B, Cs of Herpesvirus Capsids. Viruses **7**:899–
571 914.

572 21. **Hellert J**, **Weidner-Glunde M**, **Krausze J**, **Lünsdorf H**, **Ritter C**, **Schulz TF**, **Lührs T**. 2015. The
573 3D structure of Kaposi sarcoma herpesvirus LANA C-terminal domain bound to DNA. Proc
574 Natl Acad Sci USA **112**:6694–6699.

575 22. **Chang YE**, **Poon AP**, **Roizman B**. 1996. Properties of the protein encoded by the UL32 open
576 reading frame of herpes simplex virus 1. J Virol **70**:3938–3946.

577 23. **Hyun HJ**, **Sohn JH**, **Ha DW**, **Ahn YH**, **Koh JY**, **Yoon YH**. 2001. Depletion of intracellular zinc
578 and copper with TPEN results in apoptosis of cultured human retinal pigment epithelial
579 cells. Invest Ophthalmol Vis Sci **42**:460–465.

580 24. **Arslan P**, **Di Virgilio F**, **Beltrame M**, **Biological RTJO**, **1985**. 1985. Cytosolic Ca2+ homeostasis
581 in Ehrlich and Yoshida carcinomas. A new, membrane-permeant chelator of heavy metals
582 reveals that these ascites tumor cell lines have …. ASBMB **260**:2719–2727.

583 25. **Golovine K**, **Uzzo RG**, **Makhov P**, **Crispen PL**, **Kunkle D**, **Kolenko VM**. 2008. Depletion of
584 intracellular zinc increases expression of tumorigenic cytokines VEGF, IL-6 and IL-8 in
585 prostate cancer cells via NF-κB-dependent pathway. Prostate **68**:1443–1449.

586 26. **Pavlova S**, **Feederle R**, **Gartner K**, **Fuchs W**, **Granzow H**, **Delecluse HJ**. 2013. An Epstein-Barr
587 Virus Mutant Produces Immunogenic Defective Particles Devoid of Viral DNA. J Virol
588 **87**:2011–2022.

589 27. **Juillard F**, **Tan M**, **Li S**, **Kaye KM**. 2016. Kaposi's Sarcoma Herpesvirus Genome Persistence
590 **7**:1883–1815.

591 28. **Varmuza SL**, **Smiley JR**. 1985. Signals for site-specific cleavage of HSV DNA: maturation
592 involves two separate cleavage events at sites distal to the recognition sequences. Cell
593 **41**:793–802.

594 29. **Tong L**, **Stow ND**. 2009. Analysis of Herpes Simplex Virus Type 1 DNA Packaging Signal
595 Mutations in the Context of the Viral Genome. J Virol **84**:321–329.

596 30. **Siggers T**, **Gordan R**. 2014. Protein-DNA binding: complexities and multi-protein codes.
597 Nucleic Acids Res **42**:2099–2111.

598 31. **Yang W**. 2010. Nucleases: diversity of structure, function and mechanism. Quart Rev
599 Biophys **44**:1–93.

600 32. **Nadal M**, **Mas PJ**, **Blanco AG**, **Arnan C**, **Sola M**, **Hart DJ**, **Coll M**. 2010. Structure and
601 inhibition of herpesvirus DNA packaging terminase nuclease domain. Proc Natl Acad Sci USA
602 **107**:17059–17059.

603 33. **Nakamura H**, **Lu M**, **Gwack Y**, **Souvlis J**, **Zeichner SL**, **Jung JU**. 2003. Global Changes in
604 Kaposi's Sarcoma-Associated Virus Gene Expression Patterns following Expression of a
605 Tetracycline-Inducible Rta Transactivator. J Virol **77**:4205–4220.

606 34. **Sancak Y**, **Peterson TR**, **Shaul YD**, **Lindquist RA**, **Thoreen CC**, **Bar-Peled L**, **Sabatini DM**.
607 2008. The Rag GTPases Bind Raptor and Mediate Amino Acid Signaling to mTORC1. Science
608 **320**:1496–1501.

609 35. **Labo N**, **Miley W**, **Marshall V**, **Gillette W**, **Esposito D**, **Bess M**, **Turano A**, **Uldrick T**,
610 **Polizzotto MN**, **Wyvill KM**, **Bagni R**, **Yarchoan R**, **Whitby D**. 2014. Heterogeneity and
611 Breadth of Host Antibody Response to KSHV Infection Demonstrated by Systematic Analysis
612 of the KSHV Proteome. PLoS Pathog **10**:e1004046–11.

613 36. **Dyballa N**, **Metzger S**. 2009. Fast and Sensitive Colloidal Coomassie G-250 Staining for
614 Proteins in Polyacrylamide Gels. JoVE 1–5.

615

616 **Figure 1**

617 Characterization of the expression of KSHV ORF68. (A) Western blot showing the expression
618 kinetics of ORF68 relative to the early protein ORF59 and the late protein K8.1 in iSLK.BAC16
619 cells post reactivation with doxycycline (dox). GAPDH serves as a loading control. (B) Anti-
620 ORF68 western blot of lysates of HEK293T cells transfected with plasmids expressing either the
621 extended (ORF68-Extended) or shorter form of ORF68, next to lysates of lytically reactivated
622 iSLK.BAC16 and TREx-BCBL1 cells. Different amounts of lysate were loaded in each lane to
623 account for differing ORF68-expression levels. (C) Diagram showing the genomic locus of
624 ORF68, showing the two annotated forms, which differ by a 78 amino acid (aa) N-terminal
625 extension.

626

627 **Figure 2**

628 ORF68 localizes within replication compartments and in cytoplasmic puncta of KSHV infected
629 cells. Reactivated and unreactivated BAC16.iSLK and TREx-BCBL1 cells were stained with
630 antibodies to ORF68 (red), the viral replication compartment marker ORF59 (green), and DAPI
631 (blue). The far-right panel shows the merged image.

632

633 **Figure 3**

634 Characterization of the ORF68-deficient (ORF68^{PTC}) mutant virus. (A) Diagram depicting the
635 genetic locus of ORF68 and the mutations inserted into the ORF68^{PTC} virus. (B) Western blots
636 showing expression of the early ORF59 protein and the late K8.1 protein in WT, ORF68^{PTC}, and
637 ORF68^{PTC}-MR viruses. Histone H3 served as a loading control. (C) DNA replication was measured

638 by qPCR of the viral genome before and after induction of the lytic cycle. (D) Progeny virion
639 production was assayed by supernatant transfer and flow cytometry of target cells.
640
641 **Figure 4**
642 ORF68^{PTC} virus displays a genome cleavage defect. (A) Diagram depicting the DNA cleavage
643 assay protocol and the expected TR DNA laddering phenotype (or lack thereof) upon infection
644 with WT or ORF68^{PTC} virus. (B) Southern blot of the PstI-HF digested DNA with a TR probe from
645 cells infected with WT, ORF68^{PTC}, or ORF68^{PTC}-MR virus.
646
647 **Figure 5**
648 Transmission electron microscopy of WT and ORF68^{PTC} KSHV-infected cells. (A) Representative
649 images of the nuclei of iSLK cells infected with WT or ORF68^{PTC} KSHV. Boxed regions are shown
650 to the right at higher magnification to better visualize virion morphology. (B) Representative
651 images of individual capsids observed in iSLK cells infected with WT or ORF68^{PTC} KSHV, grouped
652 by their maturation stage. Only B-capsids were observed in cells infected with ORF68^{PTC} KSHV.
653
654 **Figure 6**
655 Purification of recombinant ORF68 from transiently transfected HEK293T cells. (A) Collodial
656 coomassie-stained gel demonstrating the purity and molecular weight (~52 kDa) of ORF68
657 eluted from the s200 gel filtration column. Fractions containing ORF68 were pooled,
658 concentrated, and dialyzed into storage buffer; a sample of which was loaded in the final lane.

659 (B) Absorbance trace of the s200 gel filtration column, measured at 280 nm. The first peak
660 represents the void elution at 45.52 ml and the second peak represents ORF68 at 60.35 ml.
661
662 **Figure 7**
663 Purified recombinant ORF68 shows robust DNA binding and is associated with nuclease activity.
664 (A) Representative EMSA showing increasing amounts of ORF68 binding to the subunit-length
665 TR DNA probe. (B) Binding curve of ORF68 to DNA derived from quantification of three
666 technical replicates of the EMSA, yielding an observed K_d of (53.34 ± 2.11) nM with a Hill
667 coefficient of 1.88 ± 0.12. (C) Nuclease assay with increasing amounts of ORF68, incubated with
668 an ~800bp TR probe in the presence or absence of EDTA. (D) Analysis of TR probe degradation
669 in the presence of purified ORF68 upon addition of the indicated metal. (E) Gel comparing
670 degradation of the TR probe in the presence of purified ORF68 or DNaseI +/- 1mM TPEN or 50
671 mM EDTA.

Figure 1

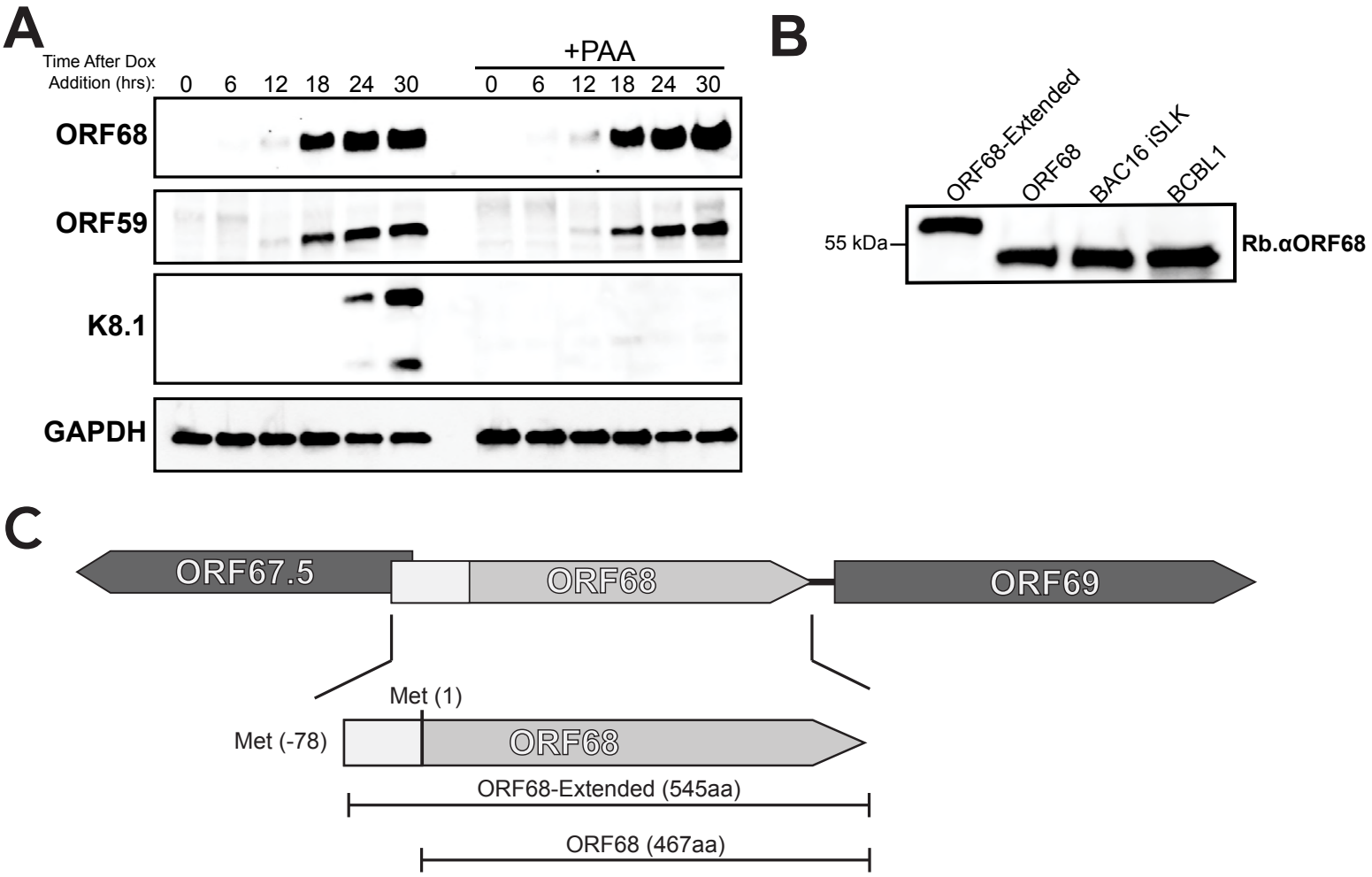
A
Time After Dox Addition (hrs):
0 6 12 18 24 30
+PAA
0 6 12 18 24 30
ORF68
ORF59
K8.1
GAPDH
B
ORF68-Extended
ORF68
BAC16 iSLK
BCBL1
55 kDa
Rb.αORF68
C
ORF67.5
ORF68
ORF69
Met (1)
Met (-78)
ORF68
ORF68-Extended (545aa)
ORF68 (467aa)

Figure 2

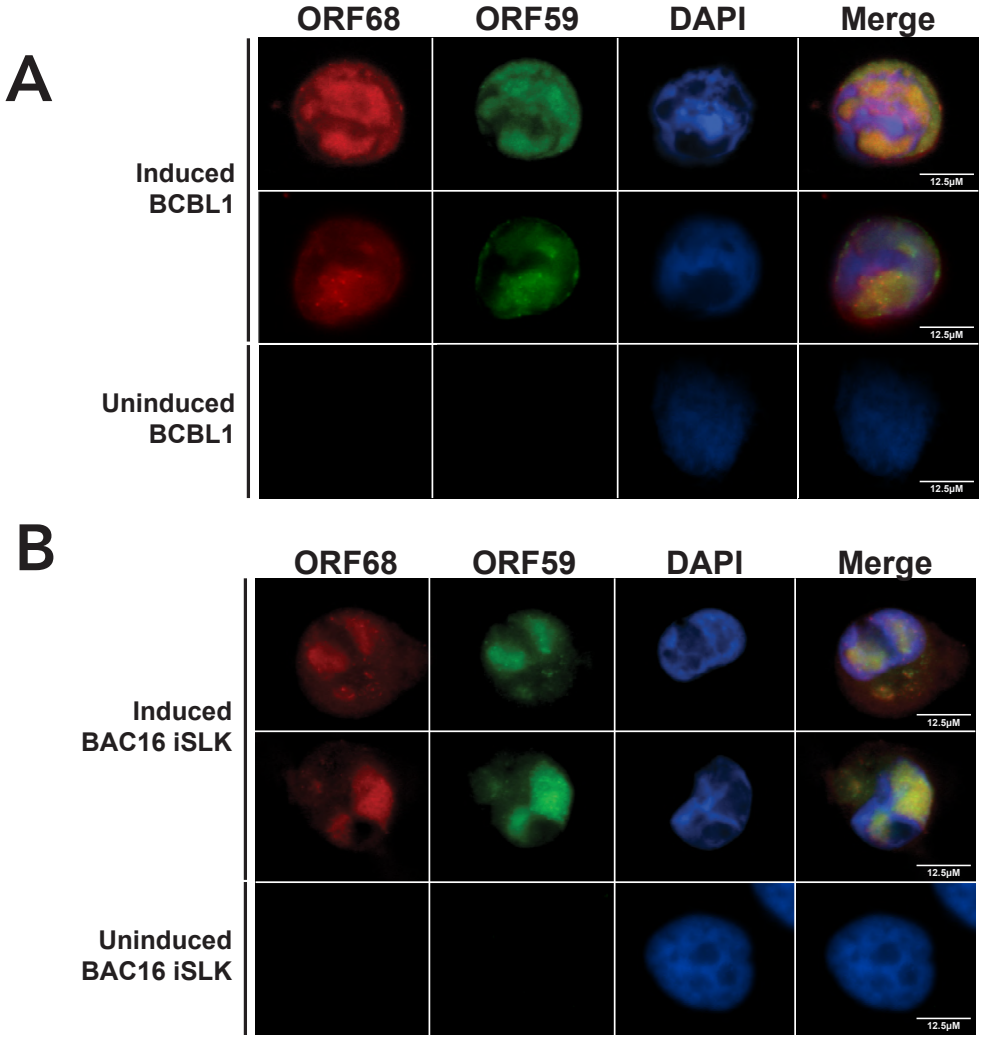
A
ORF68
ORF59
DAPI
Merge
Induced BCBL1
Uninduced BCBL1
12.5μM
B
ORF68
ORF59
DAPI
Merge
Induced BAC16 iSLK
Uninduced BAC16 iSLK
12.5μM

Figure 3

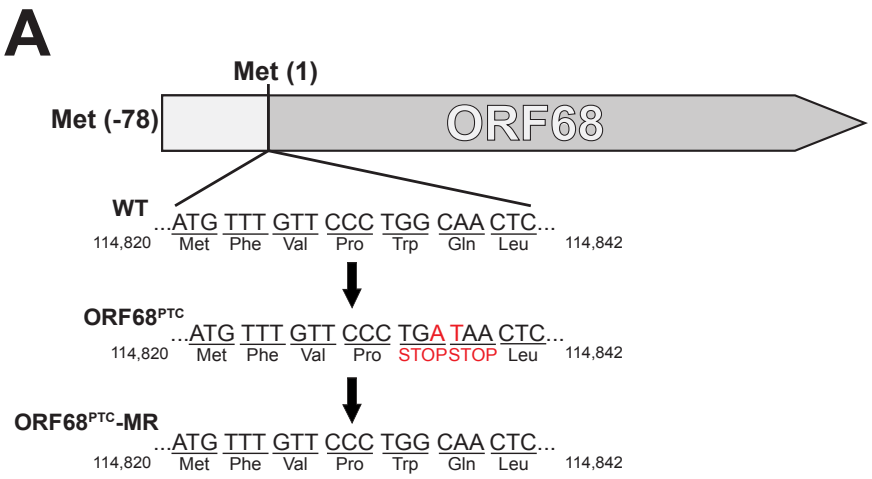
A
Met (1)
Met (-78)
ORF68
WT
...ATG TTT GTT CCC TGG CAA CTC...
114,820 Met Phe Val Pro Trp Gln Leu 114,842
ORF68PTC
...ATG TTT GTT CCC TGA TAA CTC...
114,820 Met Phe Val Pro STOP STOP Leu 114,842
ORF68PTC-MR
...ATG TTT GTT CCC TGG CAA CTC...
114,820 Met Phe Val Pro Trp Gln Leu 114,842

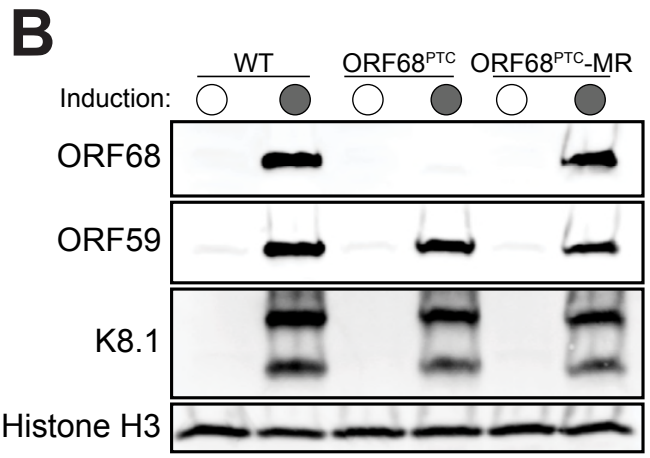
B
WT
ORF68PTC
ORF68PTC-MR
Induction:
ORF68
ORF59
K8.1
Histone H3

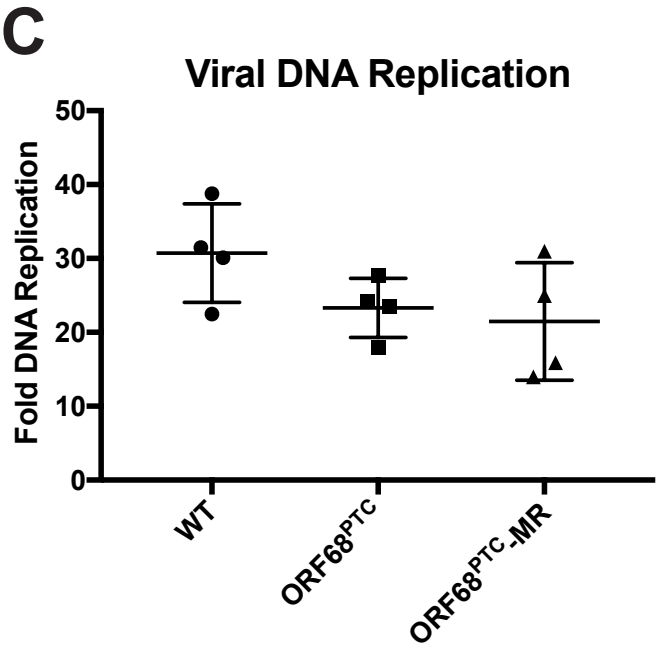
C
Viral DNA Replication
Fold DNA Replication
50
40
30
20
10
0
WT
ORF68PTC
ORF68PTC-MR

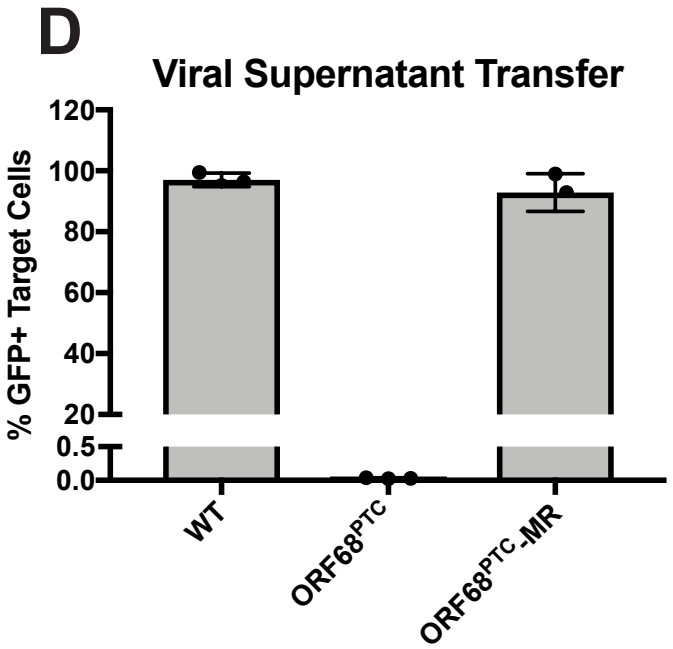
D
Viral Supernatant Transfer
% GFP+ Target Cells
120
100
80
60
40
20
0.5
0.0
WT
ORF68PTC
ORF68PTC-MR

Figure 4

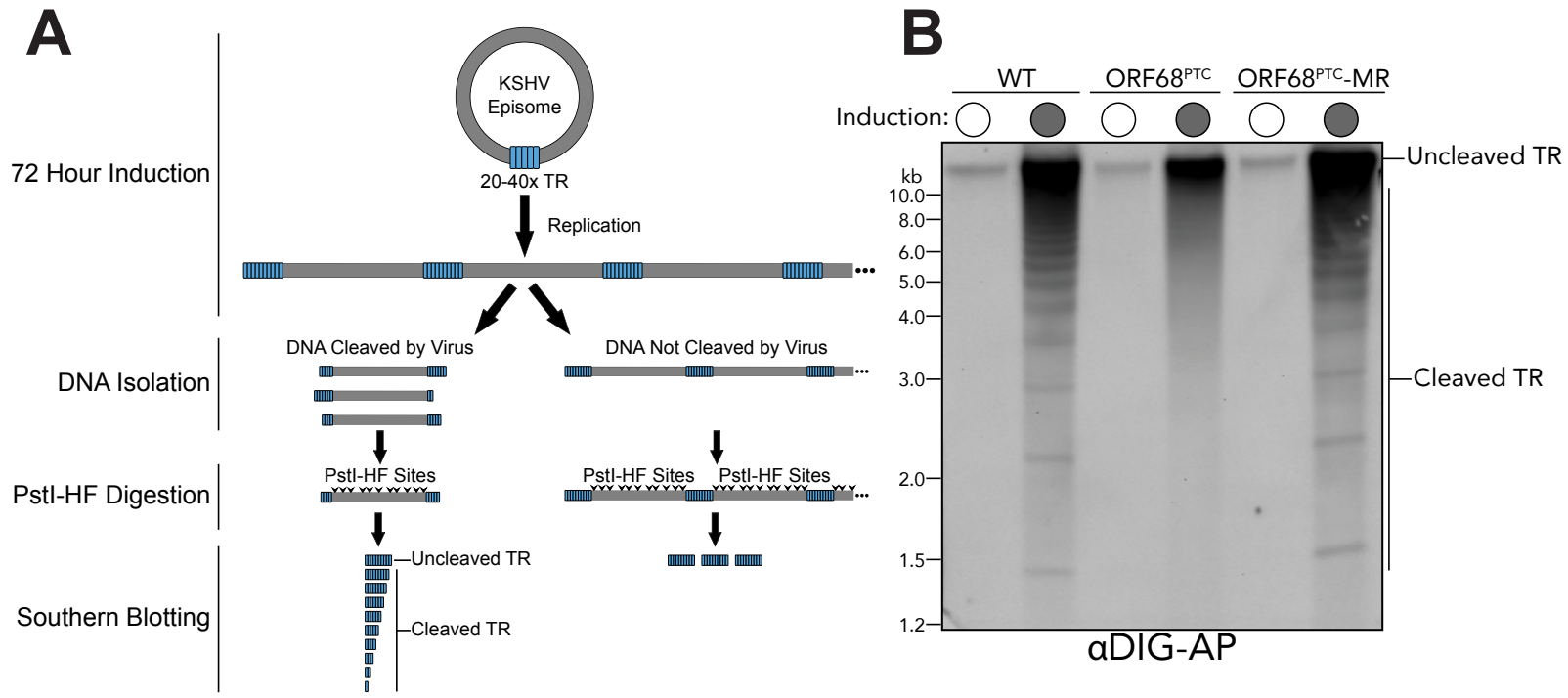
A
72 Hour Induction
KSHV Episome
20-40x TR
Replication
DNA Isolation
DNA Cleaved by Virus
DNA Not Cleaved by Virus
PstI-HF Digestion
PstI-HF Sites
PstI-HF Sites
PstI-HF Sites
Southern Blotting
Uncleaved TR
Cleaved TR
B
WT
ORF68PTC
ORF68PTC-MR
Induction:
kb
10.0
8.0
6.0
5.0
4.0
3.0
2.0
1.5
1.2
Uncleaved TR
Cleaved TR
αDIG-AP

Figure 5

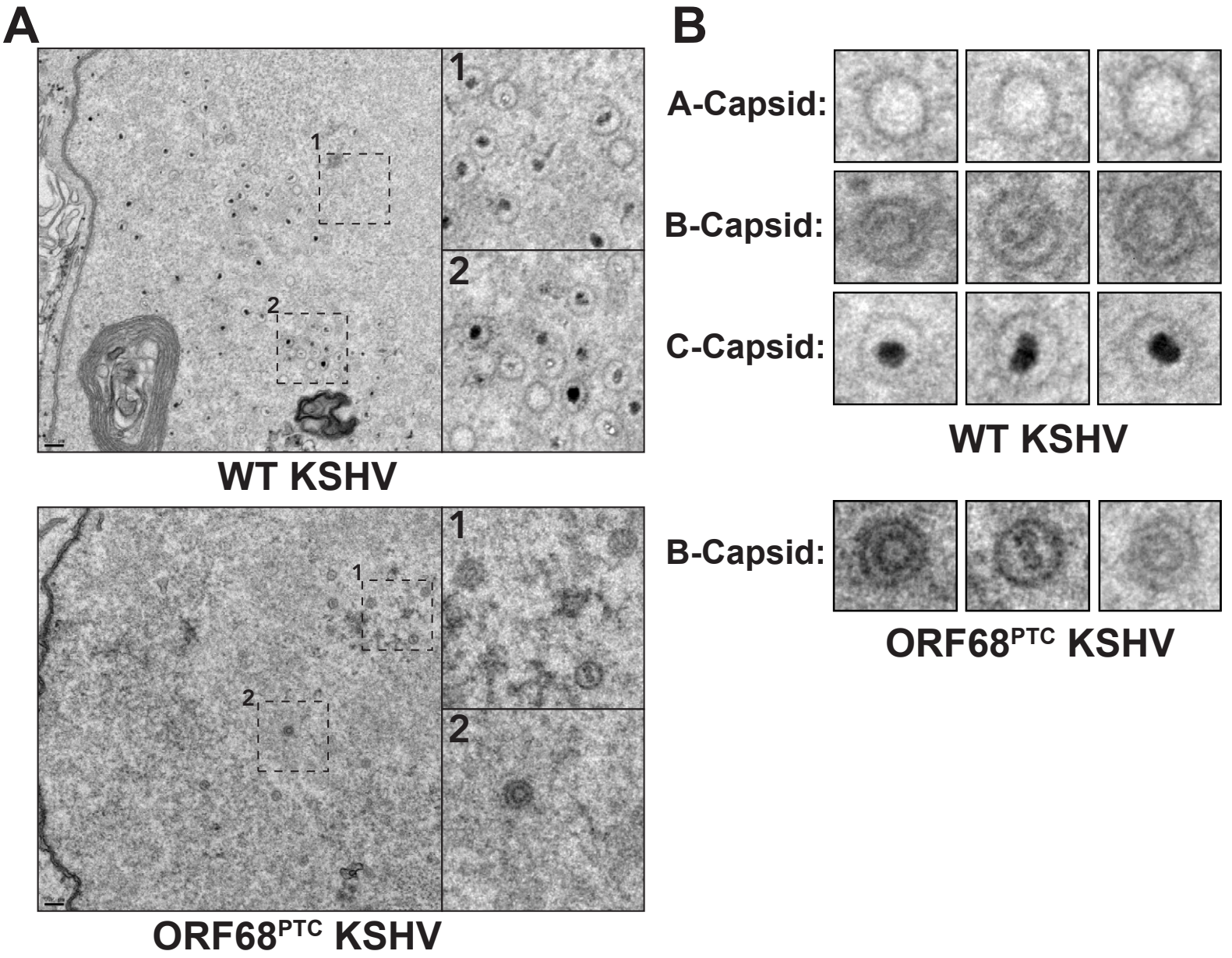
A
1
2
WT KSHV
ORF68PTC KSHV
B
A-Capsid:
B-Capsid:
C-Capsid:
WT KSHV
B-Capsid:
ORF68PTC KSHV

Figure 6

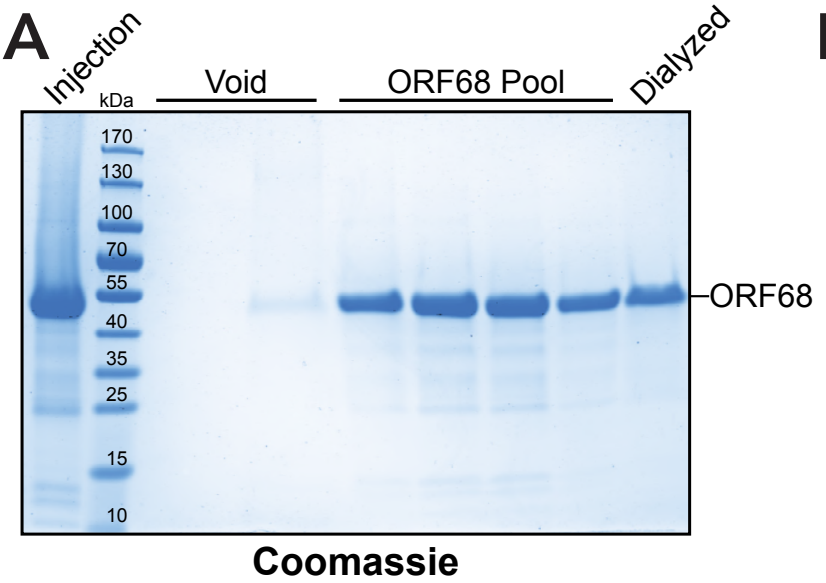
A
Injection
Void
ORF68 Pool
Dialyzed
kDa
170
130
100
70
55
40
35
25
15
10
ORF68
Coomassie

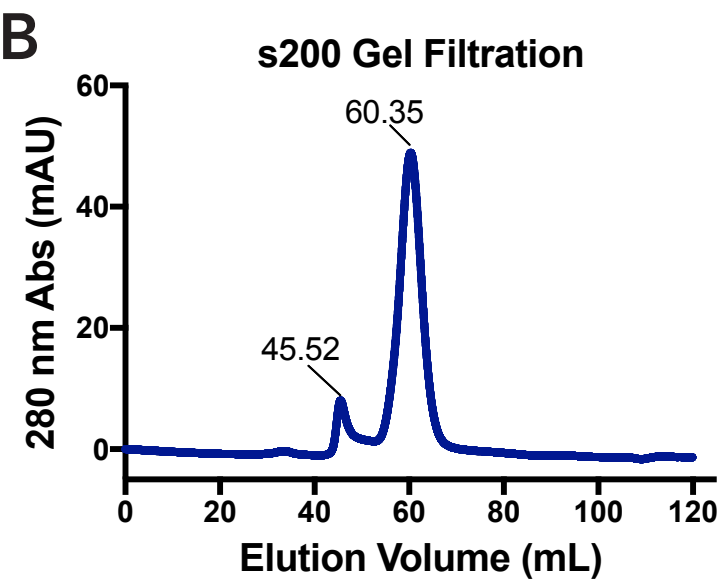
B
s200 Gel Filtration
60.35
45.52
280 nm Abs (mAU)
0
20
40
60
0
20
40
60
80
100
120
Elution Volume (mL)

Figure 7

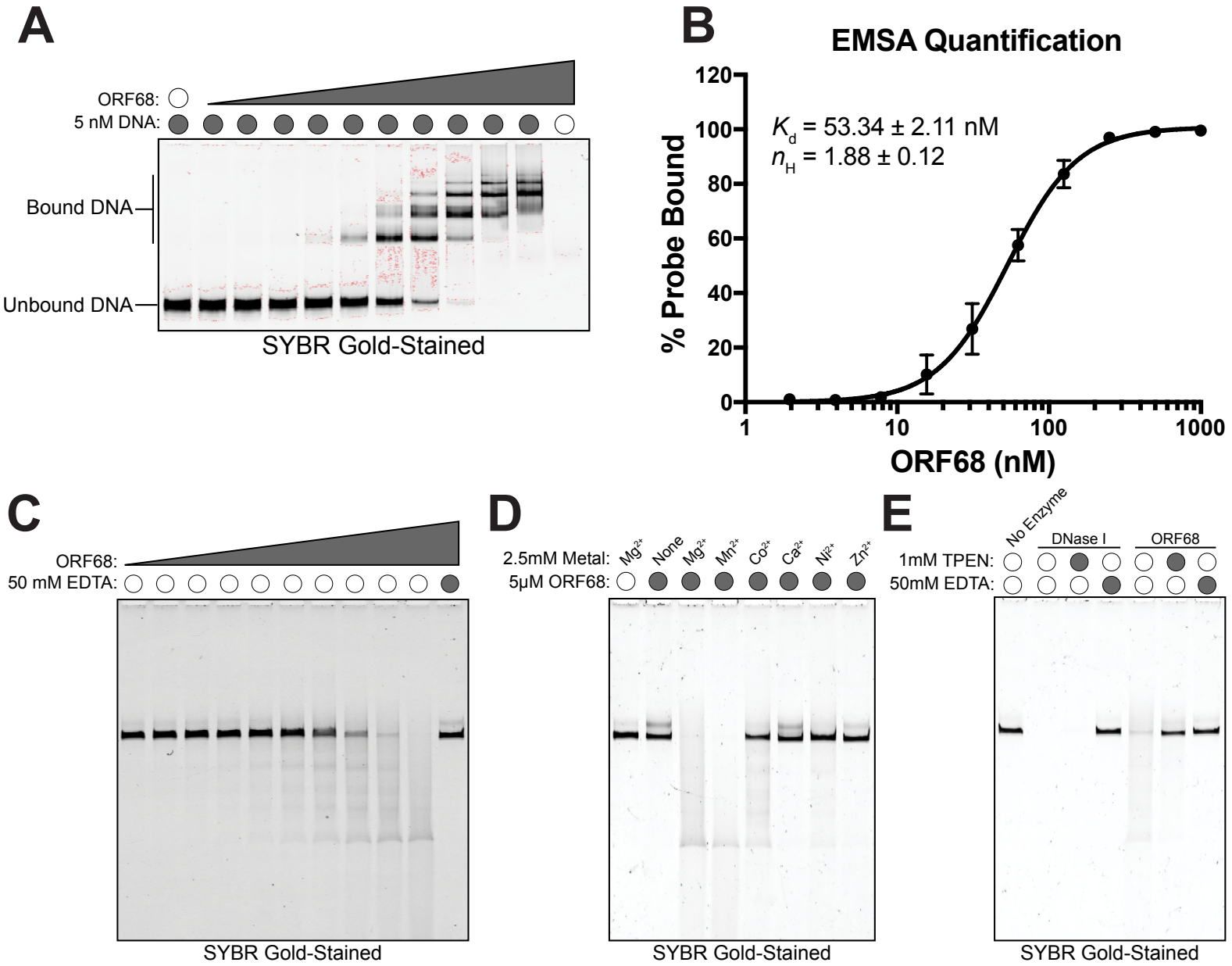
A
ORF68:
5 nM DNA:
Bound DNA
Unbound DNA
SYBR Gold-Stained
B
EMSA Quantification
K_d = 53.34 ± 2.11 nM
n_H = 1.88 ± 0.12
% Probe Bound
0
20
40
60
80
100
120
1
10
100
1000
ORF68 (nM)
C
ORF68:
50 mM EDTA:
SYBR Gold-Stained
D
2.5mM Metal:
5μM ORF68:
Mg^{2+}
None
Mg^{2+}
Mn^{2+}
Co^{2+}
Ca^{2+}
Ni^{2+}
Zn^{2+}
SYBR Gold-Stained
E
No Enzyme
DNase I
ORF68
1mM TPEN:
50mM EDTA:
SYBR Gold-Stained